

# Low $Q^2$ measurements of the proton form factor ratio $\mu_p G_E/G_M$

G. Ron,<sup>1,2,3</sup> X. Zhan,<sup>4</sup> J. Glistler,<sup>5,6</sup> B. Lee,<sup>7</sup> K. Allada,<sup>8</sup> W. Armstrong,<sup>9</sup> J. Arrington,<sup>10</sup> A. Beck,<sup>4,11</sup> F. Benmokhtar,<sup>12</sup> B.L. Berman,<sup>13</sup> W. Boeglin,<sup>14</sup> E. Brash,<sup>15</sup> A. Camsonne,<sup>11</sup> J. Calarco,<sup>16</sup> J. P. Chen,<sup>11</sup> Seonho Choi,<sup>7</sup> E. Chudakov,<sup>11</sup> L. Coman,<sup>17</sup> B. Craver,<sup>17</sup> F. Cusanno,<sup>18</sup> J. Dumas,<sup>19</sup> C. Dutta,<sup>8</sup> R. Feuerbach,<sup>11</sup> A. Freyberger,<sup>11</sup> S. Frullani,<sup>18</sup> F. Garibaldi,<sup>18</sup> R. Gilman,<sup>19,11</sup> O. Hansen,<sup>11</sup> D. W. Higinbotham,<sup>11</sup> T. Holmstrom,<sup>20</sup> C.E. Hyde,<sup>21</sup> H. Ibrahim,<sup>21</sup> Y. Ilieva,<sup>13</sup> C. W. de Jager,<sup>11</sup> X. Jiang,<sup>19</sup> M. Jones,<sup>11</sup> A. Kelleher,<sup>20</sup> E. Khrosinkova,<sup>22</sup> E. Kuchina,<sup>19</sup> G. Kumbartzki,<sup>19</sup> J. J. LeRose,<sup>11</sup> R. Lindgren,<sup>17</sup> P. Markowitz,<sup>14</sup> S. May-Tal Beck,<sup>4,11</sup> E. McCullough,<sup>5</sup> M. Meziane,<sup>20</sup> Z.-E. Meziani,<sup>9</sup> R. Michaels,<sup>11</sup> B. Moffit,<sup>20</sup> B.E. Norum,<sup>17</sup> Y. Oh,<sup>7</sup> M. Olson,<sup>23</sup> M. Paolone,<sup>24</sup> K. Paschke,<sup>17</sup> C. F. Perdrisat,<sup>20</sup> E. Piassetzky,<sup>25</sup> M. Potokar,<sup>26</sup> R. Pomatsalyuk,<sup>27,11</sup> I. Pomerantz,<sup>25</sup> A. Puckett,<sup>4</sup> V. Punjabi,<sup>28</sup> X. Qian,<sup>29</sup> Y. Qiang,<sup>4</sup> R. Ransome,<sup>19</sup> M. Reyhan,<sup>19</sup> J. Roche,<sup>30</sup> Y. Rousseau,<sup>19</sup> A. Saha,<sup>11</sup> A.J. Sarty,<sup>5</sup> B. Sawatzky,<sup>17,9</sup> E. Schulte,<sup>19</sup> M. Shabestari,<sup>17</sup> A. Shahinyan,<sup>31</sup> R. Shneur,<sup>25</sup> S. Širca,<sup>32,26</sup> K. Slifer,<sup>17</sup> P. Solvignon,<sup>10</sup> J. Song,<sup>7</sup> R. Sparks,<sup>11</sup> R. Subedi,<sup>22</sup> S. Strauch,<sup>24</sup> G. M. Urciuoli,<sup>18</sup> K. Wang,<sup>17</sup> B. Wojtsekhowski,<sup>11</sup> X. Yan,<sup>7</sup> H. Yao,<sup>9</sup> and X. Zhu<sup>33</sup>

(The Jefferson Lab Hall A Collaboration)

<sup>1</sup>The Weizmann Institute of Science, Rehovot 76100, Israel

<sup>2</sup>Lawrence Berkeley National Lab, Berkeley, CA 94720, USA

<sup>3</sup>Racah Institute of Physics, Hebrew University of Jerusalem, Jerusalem, Israel 91904

<sup>4</sup>Massachusetts Institute of Technology, Cambridge, Massachusetts 02139, USA

<sup>5</sup>Saint Mary's University, Halifax, Nova Scotia B3H 3C3, Canada

<sup>6</sup>Dalhousie University, Halifax, Nova Scotia B3H 3J5, Canada

<sup>7</sup>Seoul National University, Seoul 151-747, Korea

<sup>8</sup>University of Kentucky, Lexington, Kentucky 40506, USA

<sup>9</sup>Temple University, Philadelphia, Pennsylvania 19122, USA

<sup>10</sup>Argonne National Laboratory, Argonne, Illinois, 60439, USA

<sup>11</sup>Thomas Jefferson National Accelerator Facility, Newport News, Virginia 23606, USA

<sup>12</sup>University of Maryland, Baltimore, Maryland, USA

<sup>13</sup>George Washington University, Washington D.C. 20052, USA

<sup>14</sup>Florida International University, Miami, Florida 33199, USA

<sup>15</sup>Christopher Newport University, Newport News, Virginia, 2360X, USA

<sup>16</sup>University of New Hampshire, Durham, New Hampshire 03824, USA

<sup>17</sup>University of Virginia, Charlottesville, Virginia 22904, USA

<sup>18</sup>INFN, Sezione Sanità and Istituto Superiore di Sanità, Laboratorio di Fisica, I-00161 Rome, Italy

<sup>19</sup>Rutgers, The State University of New Jersey, Piscataway, New Jersey 08855, USA

<sup>20</sup>College of William and Mary, Williamsburg, Virginia 23187, USA

<sup>21</sup>Old Dominion University, Norfolk, Virginia 23508, USA

<sup>22</sup>Kent State University, Kent, Ohio 44242, USA

<sup>23</sup>Saint Norbert College, Greenbay, Wisconsin 54115, USA

<sup>24</sup>University of South Carolina, Columbia, South Carolina 29208, USA

<sup>25</sup>Tel Aviv University, Tel Aviv 69978, Israel

<sup>26</sup>Institute "Jožef Stefan", 1000 Ljubljana, Slovenia

<sup>27</sup>Kharkov Institute, Kharkov 310108, Ukraine

<sup>28</sup>Norfolk State University, Norfolk, Virginia 23504, USA

<sup>29</sup>Duke University, Durham, NC 27708, USA

<sup>30</sup>Ohio University, Athens, Ohio 45701, USA

<sup>31</sup>Yerevan Physics Institute, Yerevan 375036, Armenia

<sup>32</sup>Dept. of Physics, University of Ljubljana, 1000 Ljubljana, Slovenia

<sup>33</sup>Duke University, Durham, North Carolina 27708, USA

(Dated: January 7, 2019)

We present an updated extraction of the proton electromagnetic form factor ratio,  $\mu_p G_E/G_M$ , at low  $Q^2$ . The form factors are sensitive to the spatial distribution of the proton, and precise measurements can be used to constrain models of the proton. An improved selection of the elastic events and reduced background contributions yielded a small systematic reduction in the ratio  $\mu_p G_E/G_M$  compared to the original analysis.

PACS numbers: 13.0.Gp, 13.60.Fz, 13.88.+e, 14.20.Dh

## I. INTRODUCTION

We present a detailed reanalysis of polarization transfer measurements of the proton form factor ratio

$\mu_p G_E/G_M$ . This is an update of the original analysis of this experiment [1], with improved selection of elas-

tic events and significantly reduced contamination from quasielastic events in the target windows. The new results are typically lower by  $\sim 1\%$ , with comparable or somewhat smaller statistical uncertainties.

The electric and magnetic form factors,  $G_E(Q^2)$  and  $G_M(Q^2)$ , are related to the spatial distribution of charge and magnetization in the proton. The form factors can be extracted in elastic electron-proton scattering, and mapped out as a function of the four-momentum transfer squared,  $Q^2$ , to yield the momentum-space structure of the proton. In a non-relativistic framework, these form factors are the Fourier transforms of the spatial distributions of the rest-frame charge and magnetization distributions. Relativistically, the form factors represent the Fourier transform of the Breit frame rather than the rest frame, and it is necessary to apply  $Q^2$ -dependent boost corrections to extract the rest-frame distributions. These corrections are model-dependent, and there is no consensus on how they should best be applied. Thus, while the form factors are directly related to the protons spatial distribution, these distributions cannot be extracted in a model-independent fashion.

It has been argued that the large-scale structure is not significantly impacted by these corrections because the boost corrections decrease at small  $Q^2$  values. However, this is not entirely correct. The boost corrections are proportional to  $Q^2$  at very low values of  $Q^2$ , and thus there is no correction in the limit  $Q^2 \rightarrow 0$ . However, while the *value* of the form factor at  $Q^2 = 0$  is not affected by these boost corrections, the  $Q^2$  dependence is modified, even at  $Q^2 = 0$ . The proton charge radius is typically defined as the slope of the form factor at  $Q^2 = 0$ , so while the boost corrections are small, they still have a finite impact on the radius extraction. Note that because the form factor for a point particle is  $Q^2$ -independent, the information on the internal structure is contained in the deviation of the form factor from the value at  $Q^2 = 0$ ,  $G_E(0) = 1$ ,  $G_M(0) = \mu_p$ . Thus the small boost corrections at low  $Q^2$  need to be compared to the small deviations from the  $Q^2 = 0$  value of the form factors, making the impact of even small boost corrections larger than one might expect. For a more detailed discussion see Ref. [2].

Fortunately, in most instances the presence of these model-dependent boost corrections is not an issue. While discussion of finite-size corrections in atomic physics are typically phrased in terms of the rest-frame charge distributions, these corrections can in fact be directly related to the measured form factors. For example, the extraction of the proton RMS charge radius from Lamb shift measurements in hydrogen [3] and muonic hydrogen [4] is a measure of the slope of the form factor at  $Q^2 = 0$ , rather than the true RMS of the rest-frame charge density. Similarly, corrections to the hyperfine splitting [5–7], which are related to the charge and magnetization radii of the proton, are extracted directly from the form factors. So while these are discussed in terms of the proton’s size or shape, it is not necessary to have the rest frame densities

to apply these corrections.

Recently, it has been demonstrated that the transverse densities can be extracted in a model-independent fashion [8] in the infinite momentum frame (IMF). This is a natural frame in which to work for the study of generalized parton distributions, but some features of the IMF distributions may not correspond to features in the rest-frame distributions [9, 10]. So while the Breit-frame distributions are not identical to the rest-frame distributions, they can provide an approximate, but somewhat more intuitive, picture for thinking about the distributions in the rest frame of the proton [11].

In spite of the difficulties in extracting the rest-frame charge and magnetization densities, the form factors still encode a great deal of information on the structure of the nucleon. With precision measurements of both proton and neutron form factors over a large kinematic range, they can provide significant constraints on models of the nucleon. The lack of a free neutron target and the limitations of the unpolarized cross section measurements led to significant limitations in these measurements. In particular, it was difficult to precisely separate  $G_E$  from  $G_M$  in the proton for very high or very low  $Q^2$  values, and even more difficult to separate proton and neutron contributions when attempting to extract neutron form factors from measurements on light nuclei. Polarization measurements [12–15] provide a significantly improved way to isolate the neutron form factors and to separate  $G_E$  and  $G_M$ . Initial measurements for the proton focused on the high- $Q^2$  region [16–19], which showed a significant falloff in the ratio  $\mu_p G_E/G_M$  with  $Q^2$ , in contrast to previous extractions from Rosenbluth separations [20]. The difference is now believed to be due to the contribution of two-photon exchange effects which significantly impact the extractions from the unpolarized cross section measurements but have significantly less impact on the measurements which use polarization observables [21–23]. These significantly improved measurements of  $G_E$  led to a great deal of theoretical work aimed at understanding this behavior [24–27], which showed, among other things, the importance of quark orbital angular momentum in understanding the proton structure at high momentum [28–30]. These results also had a significant impact on studies of the correlations between the spatial distribution of the quarks and the spin or momentum they carry, showing that the spherically symmetric proton is formed from a rich collection of complex overlapping structures [31].

While initial investigations focused on extending proton measurements to higher  $Q^2$ , the polarization measurements can also be used to improve the precision at lower  $Q^2$  values, and in particular improve the extraction of the magnetic form factor for very low  $Q^2$  values. The low- $Q^2$  form factors relate to the large-scale structures in the proton’s charge and magnetization distributions. As such, it has long been believed that the “pion cloud” contributions, e.g. the fluctuation of a proton into a virtual neutron- $\pi^+$  system, will be significant at low  $Q^2$ , as the mass difference means that the pion will contribute

to the large distance distribution in the bound nucleon–pion system. Such fluctuations yield small corrections to the charge distribution of the proton, but are more important in the neutron, where the charge form factor is small, with  $G_E^n \rightarrow 0$  in the limit of small  $Q^2$ . In this case, the small contribution from the fluctuation of the neutron into a proton– $\pi^-$  system yields a positive charge density at the neutron core and a negative pion cloud at large distance yields a significant part of the net charge distribution.

Recently it has been suggested that such structures are present in all the nucleon form factors [32], reflecting contributions from the pion cloud of the nucleon. However, the significance of the proposed structures and their interpretation as a pion cloud effect have been much disputed. This is also the region in which parity violating electron scattering measurements [33–36] are being done, to investigate the strange-quark contributions to the proton electromagnetic structure and to determine the proton weak charge, as a constraint on physics beyond the standard model. Extracting the strange quark contributions and weak charge both rely on precise determinations of the proton form factors.

Finally, these form factors can be used to extract the proton charge and magnetization radii [37–40]. The charge radius is of particular interest at present, due to the conflicting results between Lamb shift measurements on muonic hydrogen [4] and the electron scattering results and measurements from the Lamb shift in electronic hydrogen [3]. While higher order corrections, which depend on the values of the form factors at finite  $Q^2$ , can modify the extracted radius, these corrections appear to be far too small to explain the discrepancy. A recent work [41] has proposed a possible mechanism to explain a difference between electronic and muonic probes of the proton structure, due to off-shell effects in the hadronic intermediate state in the two-photon exchange diagrams. However, while this is an area that has received a great deal of attention in the recent past, the question is still unresolved.

## II. PREVIOUS MEASUREMENTS

Since the 1960s, measurements of the unpolarized cross section for elastic e–p scattering have been used to separate  $G_E$  and  $G_M$ . The cross section is proportional to  $(\tau G_M^2 + \varepsilon G_E^2)$ , where  $\tau = Q^2/4m_p^2$ , and  $\varepsilon = (1 + 2(1 + (Q^2/4m_p^2)) \tan^2 \theta/2)^{-1}$ . By keeping  $Q^2$  fixed by varying the beam energy and scattering angle, one can vary  $\varepsilon$ , and thus perform a “Rosenbluth separation” [42] of the contributions from  $G_E$  and  $G_M$ . At high  $Q^2$ , the factor of  $\tau G_M^2$  dominates, as  $\tau$  becomes large and  $G_M^2 \gg G_E^2$  (with  $G_M/ge = \mu_p$  at  $Q^2 = 0$ ). This makes extraction of  $G_E$  difficult, as it contributes only a small, angle-dependent correction to the primary cross section contribution from  $G_M$ . Similarly, in the limit of very small  $Q^2$ , and thus very small  $\tau$ , it is difficult to isolate

$G_M$ , except in the limit where  $\varepsilon \rightarrow 0$ , i.e. scattering angle  $\rightarrow 180^\circ$ .

Polarization measurements are sensitive to the ratio  $G_E/G_M$ , and thus, when combined with cross section measurements, can cleanly separate the electric and magnetic form factors, no matter how small their contribution to the cross section becomes. It has been known for some time [12–15] that measurements of polarization observables would provide a powerful alternative to Rosenbluth separation measurements, but only in the last decade or so have the high polarization, high intensity electron beams been available, combined with polarized nucleon targets or high efficiency nucleon recoil polarimeters [25, 26].

The first such measurements for the proton [16, 43] showed a decrease in  $\mu_p G_E/G_M$  with  $Q^2$ , which differed from the existing Rosenbluth separation measurements, which showed approximate form factor scaling, i.e.  $\mu_p G_E/G_M \approx 1$ . This discrepancy appeared to be larger than could be explained even accounting for the scattering in the previous Rosenbluth measurements [20]. A measurement using a modified Rosenbluth extraction technique [44] was able to extract the ratio  $\mu_p G_E/G_M$  with comparable precision to the polarization measurements, and showed a clear discrepancy, well outside of the experimental systematics for either technique. Experiments extending polarization measurements to higher  $Q^2$  show a continued decrease of  $\mu_p G_E/G_M$  with  $Q^2$  [17, 19].

It was suggested that the two-photon exchange (TPE) correction may be able to explain the discrepancy between the two techniques [21]. While these corrections are expected to be of order  $\alpha_{EM} \approx 1\%$ , they can have a very similar  $\varepsilon$  dependence to the contribution from  $G_E$ . Because the contribution to  $G_E$  is small at large  $Q^2$ , a TPE correction of a few percent could still be significant to the extraction of  $G_E$ . It was estimated that a TPE contribution of  $\sim 5\%$ , with a linear  $\varepsilon$  dependence, could explain the difference [21, 45], and early calculations suggested effects of a few percent, with just such a linear  $\varepsilon$ -dependence [46, 47]. These corrections should also modify the polarized cross section measurements, but it should be a percent-level correction in the extraction of  $G_E/G_M$ , as there is no equivalent amplification of the effect. Including the best hadronic calculations available yields consistency between the two techniques, and good separation of  $G_E$  and  $G_M$  up to high  $Q^2$  [22]. Comparisons of electron–proton and positron–proton scattering can be used to isolate TPE contributions [48], and a series of such measurements are currently planned or underway [49–51].

At low  $Q^2$  values, the TPE should be well described by the hadronic calculations, and in fact the contributions become very small for  $0.3 < Q^2 < 0.7 \text{ GeV}^2$ . While this is a region where high precision Rosenbluth separations are possible, the existing measurements in this region have relatively large uncertainties, typically larger than 3–5%, on  $\mu_p G_E/G_M$ . Measurements using polarization observables in this region can provide a significant improvement

in precision, even in this low  $Q^2$  regime. The MIT-Bates BLAST experiment made measurements of  $\mu_p G_E/G_M$  using a polarized target [52] for  $0.1 < Q^2 < 0.6 \text{ GeV}^2$ , with typical uncertainties around 2%. The updated results of this reanalysis provide an improved extraction of  $\mu_p G_E/G_M$  in this kinematic region.

### III. EXPERIMENT DETAILS

This experiment was carried out in Hall A of the Thomas Jefferson National Accelerator Facility (JLab), in the summer and fall of 2006, as part of experiment E05-103 [53]. While the experiment was focused on polarization observables in low energy deuteron photodisintegration [54], elastic electron-proton scattering measurements used to calibrate the focal plane polarimeter provided high statistics data that allowed for an improved extraction of the proton form factor ratio  $\mu_p G_E/G_M$  at low  $Q^2$ .

A polarized electron beam was incident on a cryogenic liquid hydrogen target, 10 cm in length for the 362 MeV beam energy running and 15 cm for the 687 MeV settings (the target length was misstated as 15 cm for all runs in the previous publication [1]). Elastic e-p scattering events were identified by detecting the struck proton in one of the High Resolution Spectrometers (HRS) [55]. Data were taken with a longitudinal polarization of approximately 40% and with the beam helicity flipped pseudo-randomly at 30Hz. For some settings, the scattered electron was detected in the other HRS spectrometer.

The polarization of the struck protons is measured in a focal plane polarimeter (FPP) in the proton spectrometer. Operation and analysis of events in the FPP is described in detail in Refs. [18, 55]. Analysis of the angular distribution of rescattering in the polarimeter allows us to extract the transverse polarization at the detector, which can be used to reconstruct the longitudinal and transverse (in-plane) components of the polarization of the elastically scattered protons. In the Born approximation, the ratio of these polarization components is directly related to the ratio  $G_E/G_M$ ,

$$R \equiv \frac{G_E}{G_M} = -\frac{E_0 + E'}{2m_p} \tan\left(\frac{\theta_e}{2}\right) \frac{C_x}{C_z}, \quad (1)$$

where  $C_{z,x}$  are the longitudinal and transverse components of the proton polarization,  $E_0$  is the beam energy, and  $\theta_e$  and  $E'$  are the scattered electron's angle and momentum (reconstructed from the measured proton kinematics). Because the extraction of  $\mu_p G_E/G_M$  depends on the ratio of two polarization components, knowledge of the absolute beam polarization and FPP analyzing power are not necessary, although high polarization and analyzing power improve the figure of merit of the measurement.

In the experiment, we measure the polarization not at the target, but in the spectrometer, and the asymmetry

in the rescattering is sensitive only to polarization components perpendicular to the proton direction. If we look at the central proton trajectory, where the spectrometer is well represented by a simple dipole, then the transverse component,  $C_x$ , will be unchanged, while the longitudinal component,  $C_z$ , will be precessed in the dipole field. If we chose a spin precession angle,  $\chi$ , near 90 degrees, the longitudinal and transverse polarization components at the target will yield "vertical" and "horizontal" components in the frame of the focal plane polarimeter, allowing for both to be extracted by a measurement of the azimuthal distribution of rescattering in the carbon analyzer. In the analysis, we use a detailed model of the spectrometer to perform the full spin precession, rather than taking a dipole approximation, as described in detail in Ref. [18].

TABLE I: Kinematics and FPP parameters for the measurements.  $\theta_{lab}^p$  and  $T_p$  are the proton lab angle and proton kinetic energy, respectively.  $T_{analyzer}$  is the thickness of the FPP carbon analyzer and  $\chi$  is the spin precession angle for the central trajectory. The final column shows which kinematics had single-arm (S), coincidence (C), or a combination of both (C/S).

$Q^2$ (GeV <sup>2</sup> )	$E_e$ (GeV)	$\theta_{lab}^p$ (deg)	$T_p$ (GeV)	$T_{analyzer}$ (inches)	$\chi$ (deg)	S/C
0.215	0.362	28.3	0.120	0.75	91.0	S
0.235	0.362	23.9	0.130	0.75	91.9	S
0.251	0.362	18.8	0.140	0.75	92.7	S
0.265	0.362	14.1	0.148	0.75	93.4	S
0.308	0.687	47.0	0.170	2.25	95.3	C
0.346	0.687	44.2	0.190	3.75	97.0	C&S
0.400	0.687	40.0	0.220	3.75	99.6	S
0.474	0.687	34.4	0.260	3.75	103.0	S

A follow-up experiment, JLab E08-007 [56] was proposed to make extremely high precision measurements in this kinematic regime. The measurements was run in the summer of 2008, and in the analysis of the E08-007 data, it was observed that the result was somewhat sensitive to the cuts applied to the proton kinematics when isolating elastic e-p scattering.

In the original analysis of our results [1], only the proton was detected for most kinematic settings, and the elastic scattering events were isolated using cuts on the over-determined elastic kinematics. Because the measurement was statistics limited, relatively loose cuts were applied, as little cut dependence had been observed in the two coincidence settings or in previous measurements where electrons were detected [18, 43] or in a previous work comparing singles and coincidence measurements [17]. Most of these measurements had high resolution reconstruction of both the proton and electron kinematics, and so loose cuts on the combined proton and electron kinematics provided clean isolation of the elastic peak. In addition, the previous measurements were generally at higher  $Q^2$  and so of significantly lower sta-

tistical precision, typically 3–5%, so it was difficult to make precise evaluation of the impact of tight cuts on the proton kinematics. Because in most cases the elastic events could be cleanly identified without tight cuts on the proton kinematics, this was not considered to be a significant concern.

In the analysis of the E08-007 data [56], the electron was detected in a large acceptance spectrometer with limited momentum and angle resolution. The electron detection led to significant suppression of scattering from the target windows, but the poor electron resolution required that the elastic peak be identified using cuts on the proton kinematics. Because of this, and the high statistics of the data set, it was possible to make detailed studies of the cut dependence of the result. It was found that there were small but noticeable changes in the extracted form factor ratio if the proton kinematic cuts were made too loose, even in cases where the endcap contributions were fairly small. This may be due to events where the spin precession was incorrectly calculated due to poor reconstruction of the proton vertex kinematics for events that are far out the tails of the elastic peak as defined by the proton kinematics. Therefore, we reexamined the cuts used to identify the proton events, and made a careful reevaluation of the contribution from the target endcaps.

For our measurement, applying a more restrictive cut on the elastic peak yielded small but systematic changes in the extracted form factor ratio. However, the primary effect was due to the reduction in the contribution from endcap scattering. This was typically a 3–5% contribution to the cross section, much less for the two coincidence settings, and it was difficult to apply the correction precisely. For systematic checks, we took data with the elastic peak centered on the focal plane, but also with the spectrometer momentum approximately 2% higher and lower, to map out the response of the FPP across the focal plane. Data on the Aluminum dummy targets was typically taken for only one setting, and so there was a systematic uncertainty associated with the stability of the size of the background contamination and the possible variation of the polarization transfer coefficients measured from the dummy target. In addition, while data was taken on both a 15 cm and a new 10 cm cryogenic hydrogen target, the dummy foils were for the standard cryotargets of 4 cm and 15 cm. Also, during some of our runs, fluctuations in beam position caused by problems with the position feedback system caused parts of the beam to go through both sets of dummy foils, making beam charge based corrections impossible. Finally, when the cuts used to identify elastic scattering were applied to the dummy target, the statistics available for measuring the polarization coefficients for scattering from Aluminum were very limited, and the statistical fluctuations in the Aluminum contribution were sometimes large enough to be a significant contribution to the total uncertainty, especially after accounting for the uncertainty in the measurement of the endcap contribution to the scattering.

#### IV. ANALYSIS DETAILS

For elastic scattering with an electron beam at a fixed beam energy, the complete scattering kinematics can be determined from the measurement of a single kinematic quantity, typically the angle or energy of the final state electron or proton. If two quantities are measured, then the consistency of the two kinematic variables can be used to determine if the event was associated with elastic scattering. For this analysis, we use the proton scattering angle and momentum to reconstruct the kinematics and to identify elastic events. For some kinematics, the electron was also detected, which allows for almost complete suppression of events coming from quasielastic scattering in the Aluminum entrance and exit windows of the target. To identify the elastic peak, we use the difference between the measured proton momentum and the momentum calculated for elastic scattering using the measured proton angle. The specific variable we use in  $DpKin$ , which is the momentum difference,  $p_p - p_{elastic}(\theta_p)$ , divided by the central momentum setting of the proton spectrometer. This yields a fractional momentum deviation from the expectation for elastic scattering.

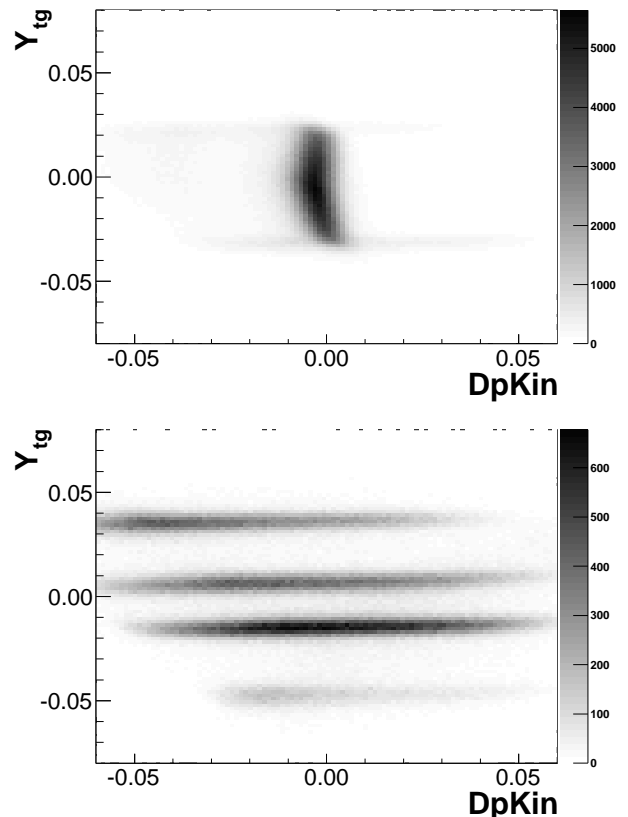


FIG. 1: Plots showing the reconstructed target position,  $Y_{tg}$  vs.  $DpKin$ , the deviation of the momentum from the expected elastic peak position, for the 10 cm liquid hydrogen target and the dummy foils.

Figure 1 shows the distribution of events versus  $DpKin$  and the reconstructed target position,  $Y_{tg}$ , as seen by the spectrometer. For the hydrogen target (top panel), there is a strong peak at  $DpKin \approx 0$ , corresponding to elastic events. At the extreme  $Y_{tg}$  values, there is a faint but broad distribution corresponding to quasielastic scattering in the endcaps. We apply a cut to  $Y_{tg}$  to remove most of the contribution from the endcap scattering, and use the measurements from the dummy target (bottom panel) to subtract the residual contribution. The measurements from the dummy target need to be normalized to the endcap scattering to subtract away the contribution from quasielastic scattering. However, note that for the spectra shown in Fig. 1, the length of the LH2 target does not match either the inner or the outer pair of foils from the dummy target. This means that the acceptance as a function of  $DpKin$  will not be identical for the endcaps and the foils in the dummy target, and this is clear for the outer foils of the dummy target, where there is a significant loss of events at extreme positive (negative) values of  $DpKin$  for the upstream (downstream) dummy foils.

Because of the difficulty in determining the normalization of the dummy target relative to the aluminum endcaps, the spectra are normalized to match the observed “super-elastic” contribution ( $DpKin > 0$ ) in the LH2 data, using only the inner foils for the dummy target, as they have a  $DpKin$  acceptance which better matches the endcaps. Figure 2 shows the spectra for the LH2 target (thick black histogram) and the dummy target (grey histogram), after the dummy target has been normalized in the region indicated by the vertical dashed lines. After normalizing the spectra in this region, we can determine the endcap contribution under the elastic peak. The region used to define elastic events in the analysis is indicated by the vertical dotted lines.

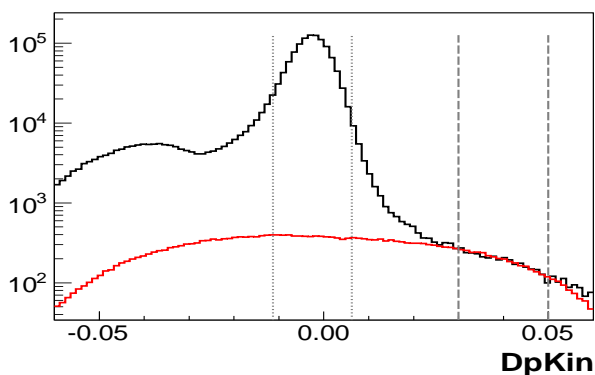


FIG. 2: (Color online) The  $DpKin$  distribution for the hydrogen target (thick black histogram) and the dummy targets (thin red histogram). The dashed vertical lines indicate the region used to normalize the dummy contribution to match the contribution from the aluminum endcaps of the hydrogen target and the vertical dotted lines indicate the part of the elastic peak used in the analysis.

Having determined the contribution from endcap scattering, we use the data from the dummy targets to determine the contributions from quasielastic scattering to the recoil polarization components  $C_x$  and  $C_z$ . If we apply the same cuts to the dummy target as we use in the analysis of the hydrogen, there is very little data left, and we can not make a reliable extraction of  $C_x$  and  $C_z$ . For the quasielastic scattering, we use all four aluminum foils and a broader cut on  $DpKin$  to determine the quasielastic values for  $C_x$  and  $C_z$ , and then assume that the coefficients are identical when looking at the central part of the quasielastic spectrum. Comparisons showed complete consistency between the extracted values of  $C_x$  and  $C_z$  when comparing the inner and outer dummy foils for all kinematics, or when comparing the central part of the quasielastic peak to the off-peak contributions.

We note that for each  $Q^2$  setting, three measurements were taken. One with the elastic peak positioned at the central momentum of the spectrometer, and two where the elastic peak was shifted up (down) by 2% in momentum. This allowed us to verify that the result was independent of the position of the events on the focal plane. However, dummy events were typically taken at only one of these three settings, and the extracted endcap contribution and quasielastic recoil polarizations taken from that measurement were applied to all three settings. Because of these limitations, we take a conservative approach and apply a 50% systematic uncertainty to the size of the endcap contribution when making the correction for these events. In addition, because we could not make a precise determination of  $C_x$  and  $C_z$  without averaging over a larger kinematic region, we apply an uncertainty to  $C_x$  and  $C_z$  of 0.02 and 0.05 respectively. Note that typical values for these polarization components in this experiment are 0.1–0.3.

In the original analysis [1], the  $Y_{tg}$  cut was loose and so there was a large contribution from endcap scattering (up to several percent of the hydrogen elastic scattering) which had to be subtracted. Because the tight cuts used on the elastic events were also applied to the Dummy spectra used to correct for endcap scattering, the statistical uncertainty on these subtractions could be very large. Therefore, fluctuations in the low statistics dummy measurements led to large uncertainties and significant fluctuations in the dummy-subtracted measurements. In the present analysis, the endcap contributions are greatly reduced, with a maximum contribution well below 1%, such that conservative systematic uncertainties assumed for the dummy normalization and polarization coefficients yield only small uncertainties in the final result. The cost was a decrease in the statistics of the hydrogen elastic events, but in the end the statistical uncertainty after the dummy subtraction was sometimes smaller, even with the tighter cuts. Note that for a few settings, additional runs were included, improving the statistics by 5–15%, but this was a small effect compared to the modified cuts.

Additionally, in the previous analysis the systematic

uncertainties from the endcap contribution were folded into the reported statistical uncertainties after the background reduction. In our new analysis, this effect has been separated out as a systematic uncertainty, somewhat reducing the reported statistical uncertainty. However, the largest effect on the uncertainty is, as noted, from the reduction of the amount of endcap contribution in the "good" events.

In addition, the estimated systematics are somewhat larger than in the previous analysis, due to a more detailed analysis of the uncertainty in the spin precession through the spectrometer, taking into account an optical model for the spectrometer magnetic field including the fringe fields.

Note that the proton energy loss, which can be significant for the low  $Q^2$  kinematics, was more carefully evaluated, leading to a change in the average  $Q^2$  for each bin compared to the original analysis [1]. Correction for the energy loss was performed on an event-by-event basis, rather than using the average values for each kinematic setting. For the 362 MeV running, where the proton was detected at small angles, applying an average energy loss is insufficient. Figure 3 shows  $DpKin$  vs.  $Y_{tg}$  for one of the 362 MeV runs with an average proton energy loss is applied to all events. Positive  $Y_{tg}$  values correspond to the front (upstream) portion of the target, where all events exit through the side of the target, and thus travel through a constant amount of hydrogen and aluminum endcap, and can be well corrected assuming a fixed energy loss. Events that exit through the downstream end of the target have reduced energy loss, as they pass through a reduced amount of material, yielding a  $Y_{tg}$ -dependent position for the elastic peak. This yields a reduced proton energy loss, and thus a higher apparent proton momentum after applying the correction for the nominal energy loss. For these kinematics, we use a  $Y_{tg}$ -dependent cut, cut corresponding to a two-sigma region around the elastic peak for each region of  $Y_{tg}$ , as indicated by the graphical cut displayed in Fig. 3.

TABLE II: Kinematic-dependent cuts applied to the data. The  $Y_{tg}$  cut is chosen to significantly suppress any contributions from the target endcap (as shown in Fig. 3).

$Q^2$ (GeV <sup>2</sup> )	$\theta_{lab}^p$ (deg)	$Y_{tg}$ cut	$\delta p/p$ cut
0.215	28.3	$-0.022 < Y_{tg} < 0.018$	$ \delta p/p  < 0.045$
0.235	23.9	$-0.022 < Y_{tg} < 0.018$	$ \delta p/p  < 0.045$
0.251	18.8	$-0.018 < Y_{tg} < 0.012$	$ \delta p/p  < 0.045$
0.265	14.1	$-0.014 < Y_{tg} < 0.010$	$ \delta p/p  < 0.045$
0.308	47.0	$-0.025 < Y_{tg} < 0.020$	$ \delta p/p  < 0.040$
0.346	44.2	$-0.025 < Y_{tg} < 0.020$	$ \delta p/p  < 0.040$
0.400	40.0	$-0.028 < Y_{tg} < 0.022$	$ \delta p/p  < 0.040$
0.474	34.4	$-0.024 < Y_{tg} < 0.020$	$ \delta p/p  < 0.040$

The kinematic-dependent cuts are detailed in Table II. In addition, several cuts were applied to all kinematics.

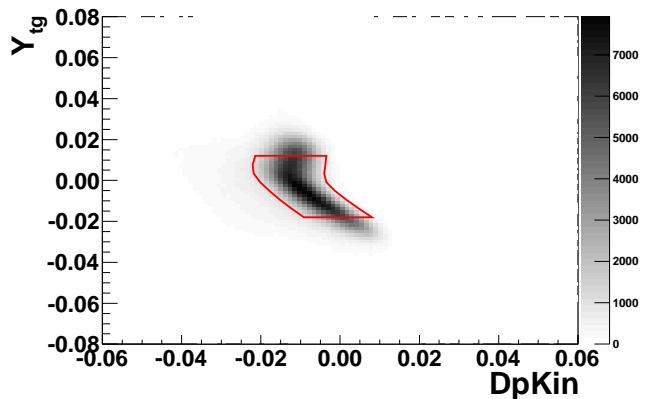


FIG. 3: (Color online) The reconstructed target position,  $Y_{tg}$  vs.  $DpKin$ , the deviation of the momentum from the expected elastic peak position. A correction for the average energy loss is applied, but there is a significant difference for events on the upstream side of the target, which exit through the side wall of the target, and events which occur nearer the downstream end of the target and have less energy loss. The band indicates the graphical cut placed on these runs, to approximate a two-sigma range for each  $Y_{tg}$  value.

A cut was applied on the out-of-plane angle,  $|\theta_{tg}| < 0.06$ , and the in-plane angle,  $|\phi_{tg}| < 0.03$ , to ensure events were inside of the angular acceptance of the spectrometer. A two-sigma cut was applied on the  $DpKin$  peak, with a  $Y_{tg}$ -dependence cut for the low energy kinematics to account for the position-dependent average energy loss as shown in Figure 3. The tracks before and after the Carbon analyzer were used to determine the scattering location and scattering angle in the analyzer. Events were required to have the secondary scattering occur within the analyzer, and angle between 5 and 50° were accepted. In addition, we apply a cone test to ensure that there is complete azimuthal acceptance in the FPP. We do this by requiring that the FPP would have accepted events with any azimuthal angle given the reconstructed vertex and scattering angle. This ensures that that any asymmetry in the acceptance or distribution of events does not lead to a difference in the scattering angle distribution for vertical and horizontal rescattering. A significant difference between the rescattering distribution for vertical and horizontal rescattering events would yield a different average analyzing power, and the analyzing power would not cancel out in the ratio of polarization components. The cone test cut ensures that the distribution of rescattering angles is independent of the azimuthal angle, so that it will drop out in the ratio, as discussed in more detail in Ref. [18].

The combination of the more restrictive cuts on the elastic events and the associated reduction in contamination due to scattering from the target windows leads to a reduction in the extracted ratio that is typically at the 1–2% level. The largest effect is due to the improved correction for endcap scattering, mainly due to

TABLE III: Systematic uncertainties. See text for details.

$Q^2$ (GeV <sup>2</sup> )	$\delta R$ (endcap)	$\delta R$ (optics)	$\delta R$ (cuts)
0.215	0.0012	0.0079	0.0141
0.235	0.0004	0.0079	0.0120
0.251	0.0003	0.0078	0.0107
0.265	0.0003	0.0076	0.0098
0.308	–	0.0091	0.0077
0.346	–	0.0086	0.0066
0.400	0.0010	0.0088	0.0056
0.474	0.0007	0.0117	0.0049

cuts which significantly reduced the size of this contribution. There is also a 1% reduction in the coincidence settings, where there are negligible endcap contributions, which is due to the tighter cuts on the proton kinematics. Tight elastic kinematics cuts using just the proton will remove events where there is a larger than average error in the reconstruction of the proton scattering angle or momentum due to multiple scattering or imperfect track reconstruction. While these errors are small, the reconstructed kinematics are used to determine the spin propagation through the spectrometer, and thus the impact of the poor reconstruction may be amplified in evaluating the spin precession.

## V. RESULTS

The results of the reanalysis are given in Table IV and shown in Figure 4, which presents the updated results along with previous measurements and a selection of fits. The updated analysis yielded a systematic decrease of  $\sim 1\%$  in the extracted ratio, except for the highest  $Q^2$  point which decreased by 5%. Note that the analyzing power has been extracted [57] from these data, but the quality of this extraction does not impact these results, as the analyzing power cancels out in the ratio of Eq. 1

The results in Fig. 4 show that the original conclusions of [1] are largely unaffected. The new results confirm the observation that  $\mu_p G_E/G_M < 1$  even for these low  $Q^2$  values, with the change from previous Rosenbluth separations being driven mainly by a change in  $G_E$ , with a smaller change in  $G_M$ . The previous hint of a local minimum near  $Q^2 = 0.35 - 0.4$  GeV<sup>2</sup> was a consequence of the point near 0.5 GeV<sup>2</sup>, and there is no longer any indication for this in our measurement. These results further support the observation that the decrease of the ratio below unity occurs at low  $Q^2$ , and thus we expect that there will be a slightly larger impact on the extraction of strange quark contributions, as discussed in the original paper [1].

Figure 5 shows the measurements compared to a set of theoretical curves. The first type of calculations are

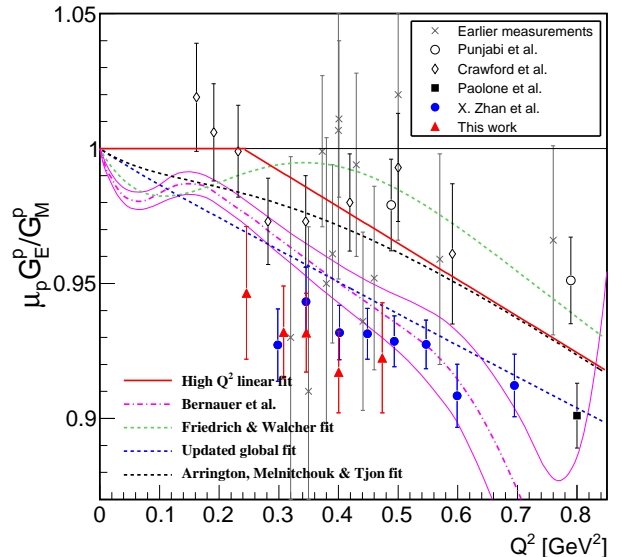


FIG. 4: (Color online) The proton form factor ratio as a function of four-momentum transfer  $Q^2$ , shown with previous extractions with total uncertainties  $\leq 3\%$ . The curves are various fits [17, 32, 40, 58], while the dot-dashed curve and associated error bands show the result of the fit to the recent Mainz measurements [39].

based on the constituent quark models, which was quite successful in describing the ground state baryon static properties. To calculate the form factors, relativistic effects need to be considered. Miller [59] performed a calculation in the light-front dynamics including the effect from the pion cloud. Boffi *et al.* [60] performed a calculation in the point form frame in the Goldstone boson exchange model with point-like constituent quarks. Faessler *et al.* [61] used a chiral quark model where pions are included perturbatively and dress the bare constituent quarks by mesons in a Lorentz covariant fashion. Another large group of calculations are based on the Vector Meson Dominance (VMD) picture, in which the scattering amplitude is written as an intrinsic form factor of a bare nucleon multiplied by an amplitude derived from the interaction between the virtual photon and a vector meson. This type of models usually involve a number of free parameters for the meson mass and coupling strength. Lomon [11, 62, 65] performed the VMD fits by including additional vector mesons and pQCD constraint at large  $Q^2$ . Belushkin *et al.* [63] performed a calculation using dispersion relation analysis with additional contribution from  $\rho\pi$  and  $K\bar{K}$  continua. More recently, de Melo *et al.* [64] performed a calculation in the light-front VMD model by considering the non-valence contribution of the nucleon state. While most of the theoretical curves are a few percent higher, the calculations of Miller [59] and de Melo *et al.* [64] generally reproduce the large deviation from 1 in this low  $Q^2$  region, emphasizing the pion cloud



TABLE IV: Experimental Results.  $R$  is given along with its statistical and systematic uncertainties. The last column (f) is the fractional contribution from scattering in the target end-caps, along with the statistical uncertainty; a 50% systematic uncertainty is also applied. The contribution is negligible for the coincidence settings. For  $Q^2 = 0.474 \text{ GeV}^2$ , dummy measurements were taken at all three sub-settings, and the range of results is given. The final entry is the average of the four low  $Q^2$  points, which are of lower statistical precision.

$Q^2$ ( $\text{GeV}^2$ )	$R = \mu_p G_E / G_M$	f (%)
0.215	$0.8250 \pm 0.0483 \pm 0.0162$	0.26(3)
0.235	$0.9433 \pm 0.0414 \pm 0.0144$	0.13(2)
0.251	$0.9882 \pm 0.0420 \pm 0.0132$	0.19(3)
0.265	$0.9833 \pm 0.0349 \pm 0.0124$	0.16(2)
0.308	$0.9320 \pm 0.0123 \pm 0.0119$	–
0.346	$0.9318 \pm 0.0098 \pm 0.0108$	$-/0.40(2)$
0.400	$0.9172 \pm 0.0109 \pm 0.0105$	0.65(4)
0.474	$0.9225 \pm 0.0160 \pm 0.0127$	0.4–0.6
0.246	$0.9465 \pm 0.0204 \pm 0.0137$	n/a

or non-valence effect. However, a deeper understanding of such mechanism is still required to explain the current data.

The reanalysis yields a small but systematic disagreement between the polarization transfer measurements and the polarized target extraction from the MIT-Bates BLAST experiment [52] at the upper range of  $Q^2$ , which is somewhat larger than the systematic uncertainties in our results. However, the new results are in consistent with the most recent polarization transfer measurement [40], and slightly below the recent analysis of Mainz cross section measurements [39], which lie between the Jefferson Lab polarization transfer data and the BLAST polarized target results. While our results and the recent E08-007 measurement [40] extraction used recoil polarization, Phase-II of E08-007 [56] will use a polarized target to make measurements of comparable or better precision for  $Q^2$  from 0.015 to 0.4, providing a check of the two techniques for  $0.25 < Q^2 < 0.4$  where there will be high-precision measurements using both techniques.

This small systematic shift of the low  $Q^2$  form factors impacts on other measurements as well. For example, it was recently pointed out [66] that the reduction in the form factor yields an agreement between studies of the asymmetry in the  $D(e,e'p)n$  reaction at low missing momentum in polarized target measurements at NIKHEF and MIT-Bates [67–69], and recent measurements at Jefferson Lab [70]. Similarly, this small shift in  $G_E$  and  $G_M$  at low  $Q^2$  modifies the expected asymmetry in parity-violating elastic electron–proton scattering, which serves as the baseline when extracting the strange-quark contribution to the proton form factors [33–36]. The effect is relatively small for any given extraction, especially at forward angles, due to a partial cancellation due to the

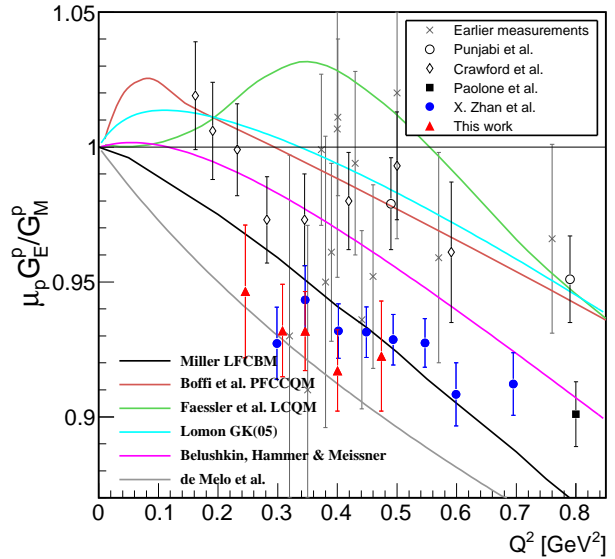


FIG. 5: (Color online) The proton form factor ratio  $\mu_p G_E / G_M$  vs.  $Q^2$ , compared to several low- $Q^2$  models. The curves shown are Millers light-front cloudy-bag model calculation [59]; Boffis point-form chiral constituent quark model calculation [60]; Fasslers light-front quark model calculation [61]; Lomons vector-meson dominance model [62]; the dispersion analysis of Belushkin, Hammer and Meissner [63]; and the model of de Melo, *et al.* [64].

changes in  $G_E$  and  $G_M$ . However, because this is a systematic correction to all such measurements, the updated form factors could have a small net contribution on the extracted strange-quark contributions.

The form factors at very low  $Q^2$  are important in both extracting the proton size and as input to other finite-size corrections in atomic physics, e.g. the Zemach radius in hyperfine splitting [5–7]. A new extraction of the proton charge radius, including these new results, was presented in Ref. [40]. This analysis yielded an RMS charge radius of  $0.875(10)$  fm, consistent with the CODATA value [3] and recent extraction from cross section measurements from Mainz [39]. Combined, these independent extractions based on the electron–proton interaction yield a radius of  $0.8772(46)$  fm [40], more than seven standard deviations from the recently published PSI muonic hydrogen Lamb shift measurement [4] of  $0.8418(7)$  fm. As yet, it is still unclear what yields this discrepancy, and extensive examinations of the corrections applied to both techniques [71–76] have found no error or inconsistency which would explain the discrepancy, although a recent work has proposed a mechanism which could yield such a discrepancy [41].

Note that while the new polarization data presented here and in Ref. [40] are somewhat high in  $Q^2$  to directly constrain the charge radius, they nonetheless play an important role in the extraction. The radius is related to

the  $Q^2$  dependence of the form factor as  $Q^2 \rightarrow 0$ , which must be fit using data over a finite  $Q^2$  range. Thus, higher order terms in the  $Q^2$  expansion need to be constrained [37] to obtain a measure of the radius. More importantly, knowledge of the relative normalization of the different cross section measurements at very low  $Q^2$  have typically been the dominant source of uncertainty in the extraction of the radius, as a shift in the normalization between large and small scattering angles can shift strength from  $G_E$  to  $G_M$  in  $Q^2$ -dependent fashion, yielding a modification of the extracted radius. By constraining the ratio of  $G_E$  to  $G_M$ , the polarization data allow for more reliable cross normalization of the different data sets.

Since the charge radius is proportional to the derivative of the form factor at  $Q^2=0$ , a new, high precision measurement of the form factor ratio at very low  $Q^2$  values [56], scheduled to run at the beginning of 2012 may shed more light on this discrepancy. At very low  $Q^2$ , measurements of the ratio  $\mu_p G_E/G_M$  can allow for a much improved extraction of the magnetic form factor at very low  $Q^2$ , as well as the magnetization radius, which have been difficult to extract precisely using unpolarized cross section measurement. This will provide improved measurements to help constrain models of the proton structure, and also provide improved information on the magnetization distribution in the proton which enters into the hyperfine splitting in hydrogen and muonic hydrogen [5–7]. These new results have also recently been incorporated in an extraction of the infinite-momentum frame charge and magnetization densities for the proton [77], where the densities are extracted along with their uncertainties, which at large distance are impacted

by the form factor uncertainties in the present  $Q^2$  range.

## VI. SUMMARY AND CONCLUSIONS

In summary, we present an updated form factor extraction from the data of Ref. [1]. We find a somewhat lower value for  $\mu_p G_E/G_M$  than the initial extraction for the entire dataset, consistent with two recent high precision measurements [39, 40]. The new analysis does not change our previous conclusion, i.e., that there is clear indication of a ratio smaller than unity, even for low  $Q^2$ , indicating the necessity of including relativistic effects in any calculation of the form factors. Both the form factors and proton charge radius extraction from various e-p scattering measurements are in agreement, and there is still a significant disagreement with the charge radius as extracted from muonic hydrogen [4].

## Acknowledgments

This work was supported by the U.S. Department of Energy, including contract DE-AC02-06CH11357, the U.S. National Science Foundation, the Israel Science Foundation, the Korea Research Foundation, the US-Israeli Bi-National Scientific Foundation, and the Adams Fellowship Program of the Israel Academy of Sciences and Humanities. Jefferson Science Associates operates the Thomas Jefferson National Accelerator Facility under DOE contract DE-AC05-06OR23177.

- 
- [1] G. Ron et al., Phys. Rev. Lett. **99**, 202002 (2007).  
 [2] J. J. Kelly, Phys. Rev. C **66**, 065203 (2002).  
 [3] P. J. Mohr, B. N. Taylor, and D. B. Newell, Rev. Mod. Phys. **80**, 633 (2008).  
 [4] R. Pohl et al., Nature **466**, 213 (2010).  
 [5] S. J. Brodsky, C. E. Carlson, J. R. Hiller, and D. S. Hwang, Phys. Rev. Lett. **94**, 022001 (2005).  
 [6] C. E. Carlson, V. Nazaryan, and K. Griffioen, arXiv:physics.atom-ph/0805.2603 (2008), 0805.2603.  
 [7] C. E. Carlson, V. Nazaryan, and K. Griffioen (2011), 1101.3239.  
 [8] G. A. Miller, Phys. Rev. Lett. **99**, 112001 (2007).  
 [9] G. A. Miller and J. Arrington, Phys. Rev. **C78**, 032201 (2008).  
 [10] G. A. Miller, E. Piasetzky, and G. Ron, Phys. Rev. Lett. **101**, 082002 (2008).  
 [11] C. Crawford et al., Phys. Rev. **C82**, 045211 (2010).  
 [12] A. I. Akhiezer, L. N. Rozentsweig, and I. M. Shmuskevich, Sov. Phys. JETP **6**, 588 (1958).  
 [13] N. Dombey, Rev. Mod. Phys. **41**, 236 (1969).  
 [14] R. G. Arnold, C. E. Carlson, and F. Gross, Phys. Rev. C **23**, 363 (1981).  
 [15] A. I. Akhiezer and M. P. Rekalo, Sov. Phys. Dokl. **13**, 572 (1968).  
 [16] M. K. Jones et al., Phys. Rev. Lett. **84**, 1398 (2000).  
 [17] O. Gayou et al., Phys. Rev. Lett. **88**, 092301 (2002).  
 [18] V. Punjabi et al., Phys. Rev. C **71**, 055202 (2005), Erratum-ibid. C **71**, 069902 (2005).  
 [19] A. J. R. Puckett et al., Phys. Rev. Lett. **104**, 242301 (2010).  
 [20] J. Arrington, Phys. Rev. C **68**, 034325 (2003).  
 [21] P. A. M. Guichon and M. Vanderhaeghen, Phys. Rev. Lett. **91**, 142303 (2003).  
 [22] J. Arrington, W. Melnitchouk, and J. A. Tjon, Phys. Rev. **C76**, 035205 (2007).  
 [23] C. E. Carlson and M. Vanderhaeghen, Ann. Rev. Nucl. Part. Sci. **57**, 171 (2007).  
 [24] C. E. Hyde-Wright and K. de Jager, Ann. Rev. Nucl. Part. Sci. **54**, 217 (2004).  
 [25] J. Arrington, C. D. Roberts, and J. M. Zanotti, J. Phys. **G34**, S23 (2007).  
 [26] C. F. Perdrisat, V. Punjabi, and M. Vanderhaeghen, Prog. Part. Nucl. Phys. **59**, 694 (2007).  
 [27] J. Arrington, K. de Jager, and C. F. Perdrisat (2011), \* Temporary entry \*, 1102.2463.  
 [28] A. V. Belitsky, X.-d. Ji, and F. Yuan, Phys. Rev. Lett.

- 91**, 092003 (2003).
- [29] S. J. Brodsky, J. R. Hiller, D. S. Hwang, and V. A. Karmanov, *Phys. Rev. D* **69**, 076001 (2004).
- [30] J. P. Ralston and P. Jain, *Phys. Rev. D* **69**, 053008 (2004).
- [31] G. A. Miller, *Phys. Rev. C* **68**, 022201 (2003).
- [32] J. Friedrich and T. Walcher, *Eur. Phys. J.* **A17**, 607 (2003).
- [33] D. S. Armstrong et al. (G0), *Phys. Rev. Lett.* **95**, 092001 (2005).
- [34] K. A. Aniol et al. (HAPPEX), *Phys. Lett. B* **635**, 275 (2006).
- [35] K. A. Aniol et al. (HAPPEX), *Phys. Rev. Lett.* **96**, 022003 (2006).
- [36] A. Acha et al. (HAPPEX), *Phys. Rev. Lett.* **98**, 032301 (2007).
- [37] I. Sick, *Phys. Lett. B* **576**, 62 (2003).
- [38] P. G. Blunden and I. Sick, *Phys. Rev. C* **72**, 057601 (2005).
- [39] J. C. Bernauer et al., *Phys. Rev. Lett.* **105**, 242001 (2010).
- [40] X. Zhan et al. (2011), 1102.0318.
- [41] G. Miller, A. Thomas, J. Carroll, and J. Rafelski (2011), arXiv:1101.4073.
- [42] M. N. Rosenbluth, *Phys. Rev.* **79**, 615 (1950).
- [43] O. Gayou et al., *Phys. Rev. C* **64**, 038202 (2001).
- [44] I. A. Qattan et al., *Phys. Rev. Lett.* **94**, 142301 (2005).
- [45] J. Arrington, *Phys. Rev. C* **69**, 022201(R) (2004).
- [46] P. G. Blunden, W. Melnitchouk, and J. A. Tjon, *Phys. Rev. Lett.* **91**, 142304 (2003).
- [47] Y. C. Chen, A. Afanasev, S. J. Brodsky, C. E. Carlson, and M. Vanderhaeghen, *Phys. Rev. Lett.* **93**, 122301 (2004).
- [48] J. Arrington, *Phys. Rev. C* **69**, 032201(R) (2004).
- [49] J. Arrington, D. M. Nikolenko, et al., Proposal for positron measurement at VEPP-3, nucl-ex/0408020.
- [50] W. Brooks, A. Afanasev, J. Arrington, K. Joo, B. Raue, L. Weinstein, et al., Jefferson Lab experiment E04-116.
- [51] M. Kohl, *AIP Conf. Proc.* **1160**, 19 (2009).
- [52] C. B. Crawford et al., *Phys. Rev. Lett.* **98**, 052301 (2007).
- [53] R. Gilman, A. Sarty, S. Strauch, et al., Jefferson Lab experiment E05-103.
- [54] J. Glister et al. (2010), 1003.1944.
- [55] J. Alcorn et al., *Nucl. Inst. & Meth.* **A522**, 294 (2004).
- [56] G. Ron, J. Arrington, D. Day, R. Gilman, D. Higinbotham, A. Sarty, et al., *Measurement of the Proton Elastic Form Factor Ratio at Low  $Q^2$* , Jefferson Lab Experiment Proposal E08-007 (2008).
- [57] J. Glister et al., *Nucl. Instrum. Meth.* **A606**, 578 (2009).
- [58] J. Arrington and I. Sick, *Phys. Rev. C* **76**, 035201 (2007).
- [59] G. A. Miller, *Phys. Rev. C* **66**, 032201 (2002).
- [60] S. Boffi et al., *Eur. Phys. J.* **A14**, 17 (2002).
- [61] A. Faessler, T. Gutsche, V. E. Lyubovitskij, and K. Pumsaard, *Phys. Rev. D* **73**, 114021 (2006).
- [62] E. L. Lomon (2006), nucl-th/0609020.
- [63] M. A. Belushkin, H. W. Hammer, and U. G. Meissner, *Phys. Rev. C* **75**, 035202 (2007).
- [64] J. P. B. C. de Melo, T. Frederico, E. Pace, S. Pisano, and G. Salme, *Phys. Lett.* **B671**, 153 (2009).
- [65] E. L. Lomon, *Phys. Rev. D* **64**, 035204 (2001).
- [66] D. Higinbotham, *AIP Conf.Proc.* **1257**, 637 (2010), 1001.3341.
- [67] I. Passchier, L. van Buuren, D. Szczerba, R. Alarcon, T. Bauer, et al., *Phys.Rev.Lett.* **88**, 102302 (2002).
- [68] B. D. Milbrath et al. (Bates FPP), *Phys. Rev. Lett.* **80**, 452 (1998).
- [69] B. D. Milbrath et al., *Phys. Rev. Lett.* **82**, 2221(E) (1999).
- [70] B. Hu, M. Jones, P. Ulmer, H. Arenhovel, O. Baker, et al., *Phys.Rev.* **C73**, 064004 (2006).
- [71] V. Barger, C.-W. Chiang, W.-Y. Keung, and D. Marfatia (2010), \* Temporary entry \*, 1011.3519.
- [72] U. Jentschura, *Eur.Phys.J.* **D61**, 7 (2011).
- [73] A. De Rujula, *Phys.Lett.* **B693**, 555 (2010).
- [74] I. C. Cloet and G. A. Miller, *Phys.Rev.* **C83**, 012201 (2011).
- [75] A. De Rujula, *Phys.Lett.* **B697**, 26 (2011).
- [76] M. O. Distler, J. C. Bernauer, and T. Walcher, *Phys.Lett.* **B696**, 343 (2011).
- [77] S. Venkat, J. Arrington, G. A. Miller, and X. Zhan, *Phys.Rev.* **C83**, 015203 (2011).